Theory of Flux-Flow Noise Voltage in Superconductors*

JOHN R. CLEM
Institute for Atomic Research and Department of Physics, Iowa State University, Ames, Iowa 50010
(Received 11 September 1969)

A theory of the time-dependent measured voltage and its associated power spectrum is developed for conditions of magnetic flux flow in the mixed and intermediate states of superconductors. Expressions for the measured voltage, appropriate for flux flow, are given and discussed. The case of a semi-infinite superconductor containing a single moving fluxoid is then examined as an illustrative model, and potentials and fields are calculated from a London-model description. The resulting time-dependent voltage pulses are computed and shown to depend upon the spatial configuration of the measuring circuit leads. The measured time-dependent flux-flow voltage and the power spectrum arising from an array of fluxoids are formulated and found to depend upon the measuring-circuit configuration, the internal flux distribution, the effects of pinning, and the modes of flux motion. Previous experimental results by van Gurp are interpreted as lending support under certain conditions to a description in terms of flux-line dislocation dipoles proposed by Kramer. New experiments are suggested as tests of the theory.

I. INTRODUCTION

RECENTLY, several experiments have been carried out to determine the power spectrum of the time-varying voltage produced across superconductors during the internal motion of magnetic flux.[1–3] Since these experiments yield interesting information about the nature of flux flow, we propose to develop in this paper a framework within which flux-flow noise experiments may be interpreted.

The organization of this paper proceeds as follows: In order to clarify what is meant by a measured flux-flow voltage, we define and discuss the voltage measured by a voltmeter when leads are attached to the surface of a specimen in Sec. II. Since a calculation of the required potentials and fields is prohibitively complicated for the general case, we perform a sample calculation in Sec. III for the simple case of a semi-infinite superconductor within which a single fluxoid is moving. We also calculate the measured time-dependent voltage and show that the resulting pulse shapes depend upon the spatial configuration of the measuring circuit. In Sec. IV, we express the measured time-dependent voltage as a superposition of contributions from a distribution of flux lines and compute the resulting power spectrum. Various flux distribution models are introduced to illustrate the influence of the flux distribution upon the power spectrum. Experimental results are briefly discussed. In Sec. V, we briefly describe how the methods developed in this paper may be applied to the case of pure flux flow in the intermediate state of type-I superconductors. We summarize our results and suggest several experiments in Sec. VI.

II. MEASURED VOLTAGES IN SUPERCONDUCTORS

When a time-dependent electric current passes through a metal at constant temperature, a gradient of the chemical potential per unit mass μ is produced along the length of the specimen, and a time-dependent vector potential $\mathbf{A}(\nabla\times\mathbf{A}=\mathbf{B})$ is produced. If one attaches zero-resistance leads from points a and b on the specimen surface to terminals A and B, respectively, of a sensitive voltmeter, as shown in Fig. 1, the measured voltage (the voltmeter "reading") is given by

$$V_{ab}=V_A-V_B=V_{ab}{}^S+V_{ab}{}^M, \tag{2.1}$$

where

$$V_{ab}{}^S=\Psi_a-\Psi_b \tag{2.2}$$

and

$$V_{ab}{}^M=-\frac{1}{c}\frac{\partial}{\partial t}\int_{a[C_M]}^{b}\mathbf{A}\cdot\mathbf{dl}. \tag{2.3}$$

The scalar potential Ψ, chosen to have units of electric potential, obeys $\nabla\Psi=-(m/e)\nabla\mu$, where m and $-e$ are the electronic mass and charge. The term $V_{ab}{}^S$ is the difference in this potential between the contact points a and b. The term $V_{ab}{}^M$, involving the line integral over the path C_M from a to b along the leads and through the voltmeter, depends upon the spatial configuration of the measuring circuit.

Alternatively, by application of Faraday's Law, we may express V_{ab} in terms of the time rate of change of magnetic flux through the measuring circuit:

$$V_{ab}=\int_{a[C_S]}^{b}\mathbf{E}'\cdot\mathbf{dl}-\frac{1}{c}\frac{\partial}{\partial t}\Phi_{MS}, \tag{2.4}$$

where

$$\mathbf{E}'=-\nabla\Psi-(1/c)\partial\mathbf{A}/\partial t \tag{2.5}$$

is a gauge-invariant generalization of the chemical potential gradient,[4] C_S is any convenient path from a to b along the specimen surface, and

$$\Phi_{MS}=\int_{S_{MS}}\mathbf{B}\cdot\hat{n}dS \tag{2.6}$$

is the magnetic flux through the surface S_{MS} bounded by paths C_M and C_S in the direction of the unit normal

* Work was performed in the Ames Laboratory of the U. S. Atomic Energy Commission. Contribution No. 2609.
[1] D. J. van Ooijen and G. J. van Gurp, Philips Res. Rept. **21**, 343 (1966).
[2] G. J. van Gurp, Phys. Rev. **166**, 436 (1968).
[3] G. J. van Gurp, Phys. Rev. **178**, 650 (1969).
[4] Y. B. Kim and M. J. Stephen, in *Superconductivity*, edited by R. D. Parks (Marcel Dekker, Inc., New York, 1969), Vol. II, Chap. 19, p. 1133.

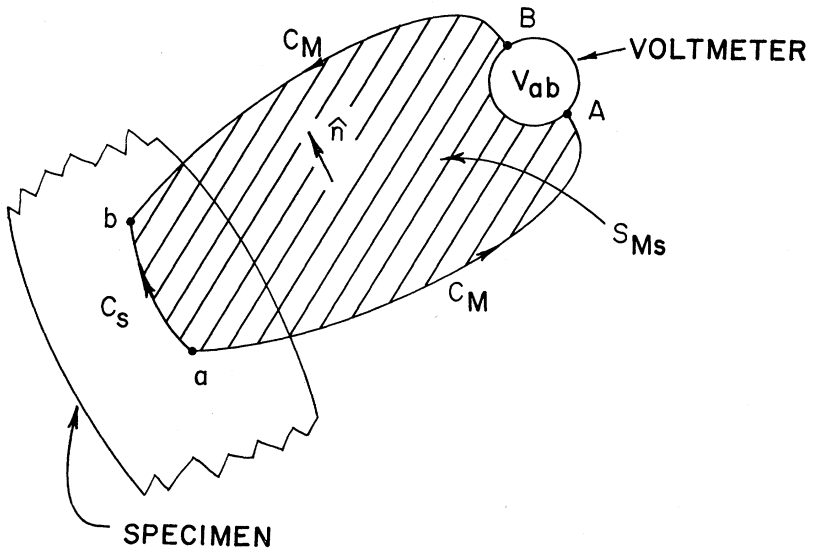

FIG. 1. Schematic voltage measuring circuit attached to a specimen at points a and b.

$\hat{n}$ shown in Fig. 1. The measured voltage V_{ab} is of course independent of the path C_S chosen by Faraday's Law, since any change in the first term on the right-hand side of Eq. (2.4) is compensated by a corresponding change in the second.

We are presently interested in the case of a superconducting metal specimen containing magnetic flux in the form of quantized vortex lines or normal domains. We employ the local London model in which the superfluid velocity $\mathbf{v}_s$ obeys[5]

$$d\mathbf{v}_s/dt = -\nabla\mu_0 - (e/m)[\mathbf{E}+(\mathbf{v}_s\times\mathbf{B})/c], \quad (2.7)$$

where μ_0 is the chemical potential per unit mass in the absence of currents or fields. Making use of the following expressions:

$$d\mathbf{v}_s/dt = \partial\mathbf{v}_s/\partial t - \mathbf{v}_s\times(\nabla\times\mathbf{v}_s) + \nabla v_s^2/2, \quad (2.8)$$

the London equation,

$$\nabla\times\mathbf{v}_s = e\mathbf{B}/mc, \quad (2.9)$$

the electric field,

$$\mathbf{E} = -\nabla\Phi - (1/c)\partial\mathbf{A}/\partial t, \quad (2.10)$$

the chemical potential per unit mass μ,[5]

$$\mu = \mu_0 + v_s^2/2 - e\Phi/m = -e\Psi/m, \quad (2.11)$$

and the electric supercurrent density $\mathbf{J}$ expressed in terms of the penetration depth λ,

$$\mathbf{J} = -n_s e\mathbf{v}_s = -(mc^2/4\pi e\lambda^2)\mathbf{v}_s, \quad (2.12)$$

we may reexpress Eq. (2.7) as

$$\mathbf{E}' = -\nabla\Psi - (1/c)\partial\mathbf{A}/\partial t = (4\pi\lambda^2/c^2)\partial\mathbf{J}/\partial t \quad (2.13)$$

in superconducting regions. In a normal vortex core or normal domain $\mathbf{E}'$ is obtained by making use of the continuity[5] of Ψ, $\mathbf{A}$, and $\mathbf{B}$ at the normal-superconducting interface.

[5] J. Bardeen and M. J. Stephen, Phys. Rev. **140**, A1197 (1965).

When the current density and magnetic field are time-independent, we see from Eq. (2.13) that $\mathbf{E}'=0$ in superconducting regions. Furthermore, if all flux-containing normal regions are surrounded by superconducting regions, $\mathbf{E}'=0$ throughout the specimen. Thus, we see from Eq. (2.4) that $V_{ab}=0$ in this case.

For the case of magnetic flux motion we may regard $\mathbf{A}$, $\mathbf{B}$, and $\mathbf{J}$ within the superconductor as prescribed as a function of time. The contribution $V_{ab}{}^S$ is calculated with the help of Eq. (2.13) to determine Ψ, and $V_{ab}{}^M$ is calculated, if necessary, with the help of Eq. (2.14) given below, to determine $\mathbf{A}$ outside the specimen. In the Coulomb gauge ($\nabla\cdot\mathbf{A}=0$), $\mathbf{A}(\mathbf{r},t)$ may be thought of as arising from the currents in the superconductor via[6]

$$\mathbf{A}(\mathbf{r},t) = \left(\frac{1}{c}\right)\int\frac{d^3r'\mathbf{J}(\mathbf{r}',t)}{|\mathbf{r}-\mathbf{r}'|}, \quad (2.14)$$

where the integration extends over the volume of the specimen. As will be demonstrated in the following sections, for the case of flux flow under constant applied current the term $V_{ab}{}^S$ may be regarded as the most important contribution to V_{ab}, since the time average of $V_{ab}{}^M$ vanishes. In fact, in some cases $V_{ab}{}^M$ may be made to vanish identically by an appropriate spatial arrangement of the voltmeter leads.

The calculation of the measured voltage V_{ab} for arbitrary specimen shape, flux distribution, and circuit geometry is quite complicated. As a beginning step, we turn our attention to the behavior of V_{ab} in the simplest model imaginable, that of an isolated singly-quantized vortex line in a semi-infinite superconductor, a model which, in spite of its simplicity, demonstrates most of the important features of time-dependent flux-flow voltages.

[6] J. D. Jackson, *Classical Electrodynamics* (John Wiley & Sons, Inc., New York, 1962), Chap. 6, p. 182.

III. ISOLATED FLUXON IN A SEMI-INFINITE SUPERCONDUCTOR

A. Vector Potential, Magnetic Induction, and Current Density

We consider a semi-infinite superconductor in the half-space $z<0$, containing a single fluxon whose axis is perpendicular to the surface $z=0$. We suppose that the fluxon intersects the surface at the origin and consider the problem of the determination of the local values of the vector potential $\mathbf{a}$, magnetic induction $\mathbf{b}$, and current density $\mathbf{j}$ if the fluxon is at rest. (We shall use lower-case symbols to denote fields associated with isolated fluxons and upper-case symbols to denote macroscopic fields obtained by superposition.) The solution of this problem is most easily accomplished using the London-model description of the vortex line,[7] in which the core radius (of the order of the coherence distance ξ) is regarded as vanishingly small by comparison with the penetration depth λ. The basic equations to be solved are Maxwell's equations, the Coulomb gauge condition $\nabla\cdot\mathbf{a}=0$, and, inside the superconductor, the first London equation,[8]

$$\mathbf{b}=-(4\pi\lambda^2/c)\nabla\times\mathbf{j}, \quad \mathbf{r}\neq 0, \tag{3.1}$$

and the analog of the Bohr-Sommerfeld quantization condition,

$$\int_S \mathbf{b}\cdot\hat{n}dS+\left(\frac{4\pi\lambda^2}{c}\right)\oint_C \mathbf{j}\cdot\mathbf{dl}=\varphi_0=\frac{hc}{2e}, \tag{3.2}$$

for any path C bounding surface S with unit normal $\hat{n}$ and encircling the vortex axis in the counterclockwise sense.

The problem defined above may be solved by the method developed by Pearl.[9] (We shall denote the solutions by the subscript 0.) In terms of cylindrical coordinates $\rho=(x^2+y^2)^{1/2}$, $\varphi=\tan^{-1}y/x$, and z, with unit vectors $\hat{\rho}=\hat{x}\cos\varphi+\hat{y}\sin\varphi$, $\hat{\varphi}=\hat{y}\cos\varphi-\hat{x}\sin\varphi$, and $\hat{z}$, the vector potential is found to be of the form $\mathbf{a}_0=a_{0\varphi}\hat{\varphi}$, where

$$a_{0\varphi}(\rho,z)=\left(\frac{\varphi_0}{2\pi\lambda^2}\right)\int_0^\infty dk\frac{J_1(k\rho)}{(k^2+\lambda^{-2})}\times\left(1-\frac{k\exp[(k^2+\lambda^{-2})^{1/2}z]}{k+(k^2+\lambda^{-2})^{1/2}}\right), \quad z\leq 0 \tag{3.3}$$

$$=\left(\frac{\varphi_0}{2\pi\lambda^2}\right)\int_0^\infty dk\frac{J_1(k\rho)}{(k^2+\lambda^{-2})^{1/2}}\times\frac{\exp(-kz)}{[k+(k^2+\lambda^{-2})^{1/2}]}, \quad z\geq 0 \tag{3.4}$$

where J_1 is the Bessel function of order unity. The local magnetic induction $\mathbf{b}_0=\nabla\times\mathbf{a}_0$ has components parallel and perpendicular to the vortex axis, $b_{0z}(\rho,z)$ and $b_{0\rho}(\rho,z)$, respectively. The current density $\mathbf{j}_0$, describing the supercurrent which flows within a penetration depth or so of the surface and the vortex axis to shield the magnetic induction from the bulk, is given by Ampere's Law, $\mathbf{j}_0=(c/4\pi)\nabla\times\mathbf{b}_0$, in the superconductor and is of the form $\mathbf{j}_0=j_{0\varphi}\hat{\varphi}$, where

$$j_{0\varphi}(\rho,z)=(c/4\pi\lambda^2)[\varphi_0/2\pi\rho-a_{0\varphi}(\rho,z)]. \tag{3.5}$$

Well above the surface of the superconductor ($z\gg\lambda$) the fields appear as if they were produced by a point monopole of magnetic charge $q_m=\varphi_0/2\pi=\hbar c/2e$ at the origin. The vector potential and magnetic induction there are given to good approximation by

$$a_{0\varphi}(\rho,z)\approx(\varphi_0/2\pi\rho)(1-z/r), \tag{3.6}$$

$$\mathbf{b}_0\approx\varphi_0\mathbf{r}/2\pi cr^3, \tag{3.7}$$

$$b_{0z}(\rho,z)\approx(\varphi_0/2\pi r^2)(z/r), \tag{3.8}$$

$$b_{0\rho}(\rho,z)\approx(\varphi_0/2\pi r^2)(\rho/r), \tag{3.9}$$

where

$$\mathbf{r}=\hat{x}x+\hat{y}y+\hat{z}z.$$

Just at the surface ($z=0$), the vector potential, magnetic induction, and current density are given by

$$a_{0\varphi}(\rho,0)=(\varphi_0/2\pi\lambda)I_1(\rho/2\lambda)K_0(\rho/2\lambda), \tag{3.10}$$

$$b_{0z}(\rho,0)=(\varphi_0/2\pi\lambda^2)[K_0(\rho/2\lambda)I_0(\rho/2\lambda)-K_1(\rho/2\lambda)I_1(\rho/2\lambda)], \tag{3.11}$$

$$b_{0\rho}(\rho,0)=(\varphi_0/2\pi\lambda^2)\times[(\lambda/\rho)^2(1-e^{-\rho/\lambda})-(\lambda/\rho)e^{-\rho/\lambda}], \tag{3.12}$$

$$j_{0\varphi}(\rho,0)=(c\varphi_0/8\pi^2\lambda^3)\times[(\lambda/\rho)-I_1(\rho/2\lambda)K_0(\rho/2\lambda)], \tag{3.13}$$

where I_n and K_n are modified Bessel functions of the first and second kind of order n.

Deep within the superconductor ($-z\gg\lambda$) the vector potential, magnetic induction, and current density are given to good approximation by

$$a_{0\varphi}(\rho,z)\approx(\varphi_0/2\pi\rho)[1-(\rho/\lambda)K_1(\rho/\lambda)], \tag{3.14}$$

$$b_{0z}(\rho,z)\approx(\varphi_0/2\pi\lambda^2)K_0(\rho/\lambda), \tag{3.15}$$

$$b_{0\rho}(\rho,z)\approx 0, \tag{3.16}$$

$$j_{0\varphi}(\rho,z)\approx(c\varphi_0/8\pi^2\lambda^2)K_1(\rho/\lambda). \tag{3.17}$$

B. Scalar Potential

If the vortex line intersects the plane $z=0$ not at the origin but at the point $\mathbf{r}_i=(x_i,y_i,0)$, and if the vortex line moves with a velocity $\mathbf{v}_i=\dot{\mathbf{r}}_i=(\dot{x}_i,\dot{y}_i,0)$, then to lowest order the vector potential, magnetic induction, and current density move rigidly along with the vortex axis and are given by the above solutions but with a lateral displacement appropriate to the new vortex

[7] P. G. de Gennes, *Superconductivity of Metals and Alloys* (W. A. Benjamin, Inc., New York, 1962), Chap. 3, p. 57.

[8] F. London, *Superfluids I, Macroscopic Theory of Superconductivity* (Dover Publications, Inc., New York, 1961), Sec. 3, p. 29.

[9] J. Pearl, J. Appl. Phys. **37**, 4139 (1966).

position:

$$\mathbf{a}(\mathbf{r},t)=\mathbf{a}_0(x-x_i, y-y_i, z), \tag{3.18}$$

$$\mathbf{b}(\mathbf{r},t)=\mathbf{b}_0(x-x_i, y-y_i, z), \tag{3.19}$$

$$\mathbf{j}(\mathbf{r},t)=\mathbf{j}_0(x-x_i, y-y_i, z). \tag{3.20}$$

The scalar potential ψ, produced in the superconductor by the vortex motion, may be calculated from Eq. (2.13), which here becomes

$$\begin{aligned}\mathbf{e}'(\mathbf{r},t)&=-\nabla\psi(\mathbf{r},t)-(1/c)\partial\mathbf{a}(\mathbf{r},t)/\partial t\\&=(4\pi\lambda^2/c^2)\partial\mathbf{j}(\mathbf{r},t)/\partial t,\end{aligned} \tag{3.21}$$

where $\mathbf{j}$ is given by Eqs. (3.20), (3.5), and (3.3). Aside from an additive constant, ψ is given by

$$\psi(\mathbf{r},t)=\boldsymbol{\varphi}_0\cdot\boldsymbol{\varrho}'\times\mathbf{v}_i/2\pi c\rho'^2, \quad z\leq 0 \tag{3.22}$$

where $\boldsymbol{\varphi}_0=\varphi_0\hat{z}$ and $\boldsymbol{\varrho}'=\hat{x}(x-x_i)+\hat{y}(y-y_i)$. The scalar potential ψ may be though of as arising from a motion-induced surface-charge density on the vortex core.[5]

C. Measured Voltage

We are now in a position to compute the resulting time-dependent voltage V_{ab} measured when voltmeter leads are connected to the superconductor surface at contact points a and b, having positions $\mathbf{r}_a=(x_a,y_a,0)$ and $\mathbf{r}_b=(x_b,y_b,0)$. According to Eqs. (2.1)–(2.3), we have

$$V_{ab}(t)=V_{ab}{}^S(t)+V_{ab}{}^M(t), \tag{3.23}$$

where

$$V_{ab}{}^S(t)=\psi(\mathbf{r}_a,t)-\psi(\mathbf{r}_b,t) \tag{3.24}$$

and

$$V_{ab}{}^M(t)=-(1/c)(\partial/\partial t)\int_{a[C_M]}^{b}\mathbf{a}(\mathbf{r},t)\cdot\mathbf{dl}. \tag{3.25}$$

The scalar potential ψ is given by Eq. (3.22) and the vector potential $\mathbf{a}$ is given by Eqs. (3.18) and (3.4).

The term $V_{ab}{}^S$ is independent of the spatial configuration of the voltmeter leads above the superconductor surface; it depends only upon the relative positions of the points a and b and the vortex axis. A convenient explicit expression for $V_{ab}{}^S$ is

$$\begin{aligned}V_{ab}{}^S=(\hbar/2e)[&\dot{x}_i(y_{bi}/\rho_{bi}{}^2-y_{ai}/\rho_{ai}{}^2)\\&-\dot{y}_i(x_{bi}/\rho_{bi}{}^2-x_{ai}/\rho_{ai}{}^2)],\end{aligned} \tag{3.26}$$

where the coordinates of the point a relative to the vortex axis are described by $x_{ai}=x_{ai}-x_i$, $y_{ai}=y_a-y_i$, and $\rho_{ai}{}^2=x_{ai}{}^2+y_{ai}{}^2$, and corresponding expressions hold for the point b. We note that $V_{ab}{}^S$ may also be written as

$$V_{ab}{}^S=(\hbar/2e)\partial(\varphi_{bi}-\varphi_{ai})/\partial t, \tag{3.27}$$

where φ_{bi} and φ_{ai} are phase angles, measured in a counterclockwise sense about the vortex axis, and $(\varphi_{bi}-\varphi_{ai})$ is the angle subtended by the points b and a at the vortex axis. Equation (3.27) may be interpreted as the Josephson condition,[10] and $(\varphi_{bi}-\varphi_{ai})$ may be regarded as the negative of the phase difference of the order parameter between the points b and a.

It is of interest to consider the case for which the velocity $\mathbf{v}_i$ is constant in time, for then $V_{ab}{}^S$ as a function of time may be written as a sum of two Lorentzians. One of the Lorentzian curves has its maximum magnitude at the time of closest approach of the vortex to point a, the other to point b. The magnitude of the time integral of each Lorentzian is equal to $\varphi_0/2c=h/4e$, but the shape of the Lorentzian becomes narrower and more sharply peaked as the distance of closest approach decreases. The magnitude of the time integral of $V_{ab}{}^S$ is either $\varphi_0/c=h/2e$, if the vortex line passes between the points a and b, or zero, if not.

A simple example of this behavior is the case of a vortex line whose intersection with the surface at time t is given by $\mathbf{r}_i=(0,vt,0)$ where the speed v in the y direction is constant. We obtain from Eq. (3.26)

$$V_{ab}{}^S(t)=\left(\frac{\hbar v}{2e}\right)\left(\frac{x_a}{x_a{}^2+(y_a-vt)^2}-\frac{x_b}{x_b{}^2+(y_b-vt)^2}\right). \tag{3.28}$$

The first term on the right-hand side of this equation is the Lorentzian corresponding to passage by point a, the second by point b. The time integral of $V_{ab}{}^S$ is easily shown to be

$$\int_{-\infty}^{\infty}V_{ab}{}^S(t)dt=(h/4e)(\mathrm{sgn}x_a-\mathrm{sgn}x_b), \tag{3.29}$$

where $\mathrm{sgn}x=x/|x|$. We note from Eq. (3.28) that $V_{ab}{}^S$ does *not* vanish when the vortex line passes outside the two contacts even though the time integral of $V_{ab}{}^S$ *does* vanish in this case.

The term $V_{ab}{}^M(t)$ given by Eq. (3.25) can be large in magnitude only when the vortex line is in the vicinity of the measuring circuit. However, the time integral of $V_{ab}{}^M$ vanishes if $|\mathbf{r}_i|\to\infty$ in the limits $t\to\pm\infty$, as is appropriate for flux flow, since

$$\begin{aligned}\int_{-\infty}^{\infty}&V_{ab}{}^M(t)dt\\&=\left(\frac{1}{c}\right)\int_{a[C_M]}^{b}[\mathbf{a}(\mathbf{r},-\infty)-\mathbf{a}(\mathbf{r},\infty)]\cdot\mathbf{dl}=0.\end{aligned} \tag{3.30}$$

The specific behavior of $V_{ab}{}^M$ depends upon the spatial configuration of the voltmeter leads above the superconductor surface.

To demonstrate some of the characteristic features of $V_{ab}(t)$ arising form the measuring circuit configuration dependence of $V_{ab}{}^M$, we consider the idealized experimental configuration shown in Fig. 2. Voltmeter leads, attached at the points a and b, extend perpendicular to the surface to points a' and b' at a height z_0 above the surface. The lead from point a then passes parallel to the surface straight over from a' to b'. From this point

[10] B. D. Josephson, Advan. Phys. 14, 419 (1965).

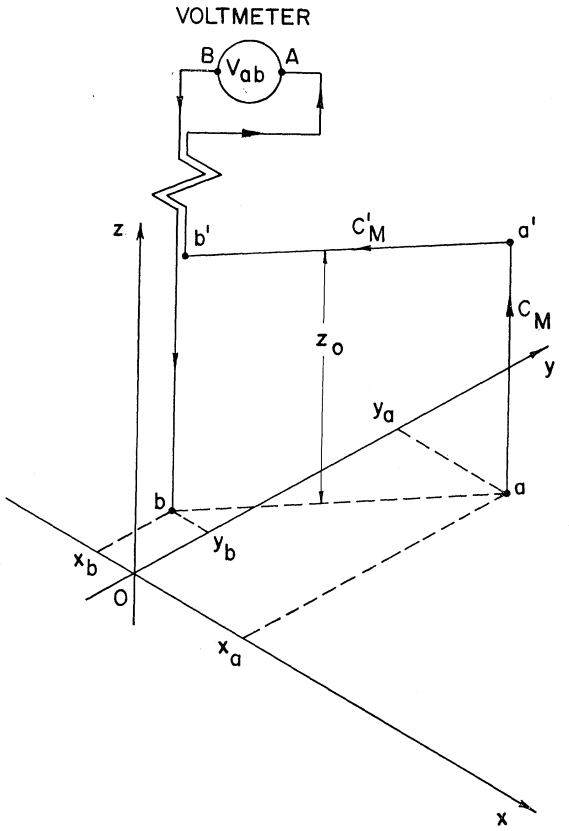

FIG. 2. Measuring circuit for which voltage pulses are calculated in the text. Voltmeter leads connect the voltmeter terminals A and B to points a and b on the superconductor surface as shown.

the two leads lie alongside each other and extend out to the voltmeter, to which they are connected at points A and B. In evaluating the integral in Eq. (3.25) for this circuit, we note that since $\mathbf{a}$ has components only parallel to the surface, its line integral vanishes along those segments of the path C_M which are perpendicular to the surface. Furthermore, the contributions along the adjacent leads extending from b' to the voltmeter cancel each other. We may assume that $\mathbf{a}$ is sufficiently small in the vicinity of the voltmeter that the contribution there may be neglected. Thus, the only contribution to $V_{ab}{}^M$ is that along the straight line path C_M' from a' at $\mathbf{r}_a' = (x_a, y_a, z_0)$ to b' at $\mathbf{r}_b' = (x_b, y_b, z_0)$, such that

$$V_{ab}{}^M(t) = -\left(\frac{1}{c}\right)\left(\frac{\partial}{\partial t}\right)\int_{a[C_M']}^{b} \mathbf{a}(\mathbf{r},t)\cdot d\mathbf{l}. \quad (3.31)$$

Let us now examine the dependence upon z_0 of the pulse shape, V_{ab} versus t, produced by a vortex line of coordinates $\mathbf{r}_i = (0, vt, 0)$ moving with constant speed v in the y direction.

In the limit as $z_0 \to \infty$, $V_{ab}{}^M$ vanishes, and we have simply $V_{ab} = V_{ab}{}^S$. The resulting voltage pulse V_{ab} versus t, given by Eq. (3.28), is shown in Fig. 3. We note that as the vortex line passes very close to one of the probe contacts, a sharply peaked voltage pulse of narrow width is produced.

For the case of arbitrary z_0, provided $z_0 \gg \lambda$, $V_{ab}{}^M$ may be computed with the aid of Eq. (3.6). The resulting value of V_{ab} in the simplifying case that $x_b = -x_a$ and $y_a = y_b = 0$ is given by

$$V_{ab}(t) = \frac{\hbar v}{e}\frac{x_a z_0}{[x_a{}^2 + z_0{}^2 + (vt)^2]^{1/2}} \times\left(\frac{1}{x_a{}^2 + (vt)^2} + \frac{1}{z_0{}^2 + (vt)^2}\right). \quad (3.32)$$

In the limit as $z_0 \to \infty$, we return to the simple Lorentzian description discussed above, except that the two Lorentzians coalesce under these conditions into a single one

$$V_{ab}(t) = (\hbar v/e) x_a/[x_a{}^2 + (vt)^2], \quad (3.33)$$

with full width at half-maximum $2x_a/v$ determined by the probe separation. This is shown in Fig. 4 as the solid curve labeled $z_0/x_a = \infty$. As z_0 decreases, the pulse shape is altered by the presence of a new characteristic length z_0 as shown by the dashed and dot-dashed curves in Fig. 4. In the limit as $z_0/x_a \to 0$, Eq. (3.32) takes on the value

$$V_{ab}(t) = (\hbar v/e) z_0/[z_0{}^2 + (vt)^2], \quad (3.34)$$

with full width at half-maximum $2z_0/v$ determined by the height z_0 of the crossing lead above the superconductor surface. The decreased width and increased peak height is seen clearly in the solid curve in Fig. 4 appropriate for the case $z_0/x_a = 0.1$.

As z_0 decreases to zero, one might suppose that the resulting voltage pulse becomes a δ-functionlike peak of infinite height and zero width. However, this is not the case, since the penetration depth λ becomes the characteristic length and $2\lambda/v$ becomes the characteristic width of the pulse. The shape of the pulse in the limit $z_0 \to 0$ is no longer Lorentzian, but, as is seen from Eq. (3.10), must be calculated numerically using modified Bessel functions. When $z_0 = 0$ and $\lambda \ll x_a$, the resulting pulse shape V_{ab} versus t is as shown in Fig. 5.

The above calculations demonstrate the usefulness of the London model, which enables the scalar and vector potentials to be calculated in a relatively simple fashion. A possible objection to this treatment is that the London model does not correctly account for the electric current and the magnetic induction in the vicinity of the superconductor surface and the vortex core. We note, however, that although ψ is calculated from the London equations which contain the single parameter λ, the resulting solution for ψ outside the core is *independent* of λ and is expressible simply in terms of the fundamental constants h and e, the vortex velocity, and the appropriate macroscopic lengths. This suggests that our result for $V_{ab}{}^S$ for probe contacts outside the core region is *exact* and that the same result

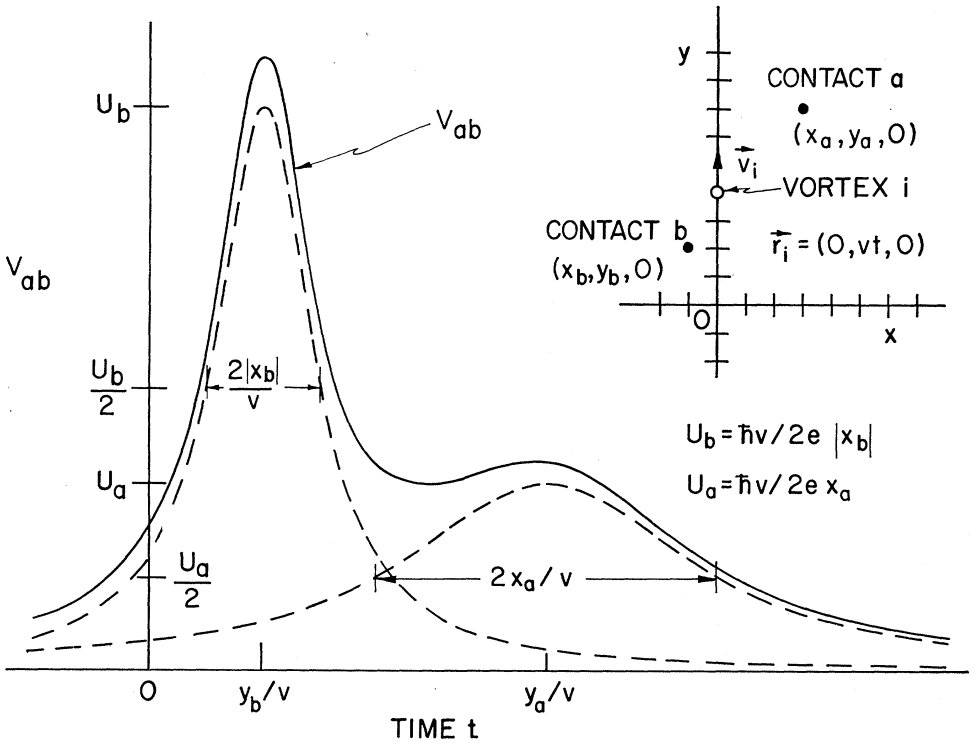

FIG. 3. Theoretical measured voltage pulse V_{ab} versus time t produced by the motion of a vortex line (magnetic flux φ_0 out of the paper) with coordinates $\mathbf{r}_i = (0, vt, 0)$ through the circuit of Fig. 2, with $z_0 = \infty$, whose relative dimensions are shown in the inset. The total pulse (solid curve) is the sum of two Lorentzians (dashed curves), as discussed in the text. The area under the curve of V_{ab} versus t is $\varphi_0/c = h/2e$.

will be obtained with any more correct theory. By the same argument, our result for $V_{ab}{}^M$ is probably also exact under these conditions, provided the voltmeter leads extend perpendicular to the superconductor surface to a height somewhat greater than λ and thereafter are kept farther than λ from the surface. We thus expect that, for most experimental geometries used for flux-flow measurements, voltage pulses may be accurately calculated by the methods used in this section.

IV. FLUX-FLOW NOISE VOLTAGE AND POWER SPECTRUM

A. Basic Formalism

In Sec. III we developed a method for determining the voltage pulse produced by a vortex line in a semi-infinite superconductor whose intersection at time t with the surface is specified by the coordinates $\mathbf{r}_i = \boldsymbol{\varrho}_i = (x_i, y_i, 0)$ and which moves through a prescribed measuring circuit. In the usual flux-flow experiment the measured voltage arises, of course, not from a single vortex line, but from a distribution of flux lines throughout the specimen. The flux-flow voltage may thus be expressed as the algebraic sum of contributions from individual vortex lines.

In order to formulate this, it is useful to note that for a given measuring circuit configuration, the contribution to the measured voltage at time t from vortex i, which we denote by $V_{ab}{}^0(\boldsymbol{\varrho}_i, \mathbf{v}_i)$, is a function *only* of $\boldsymbol{\varrho}_i(t)$ and $\mathbf{v}_i(t) = \dot{\boldsymbol{\varrho}}_i(t)$. Moreover, $V_{ab}{}^0(\boldsymbol{\varrho}_i, \mathbf{v}_i)$ may be expressed, in general, as the time derivative of a function F_{ab} which depends for a given measuring circuit only upon $\boldsymbol{\varrho}_i(t)$:

$$V_{ab}{}^0(\boldsymbol{\varrho}_i, \mathbf{v}_i) = \partial F_{ab}(\boldsymbol{\varrho}_i)/\partial t. \tag{4.1}$$

For the case of the semi-infinite superconductor F_{ab} is given by

$$F_{ab}(\boldsymbol{\varrho}_i) = -\frac{1}{c}\int_{a[C_M]}^{b} \boldsymbol{\alpha}(\mathbf{r} - \boldsymbol{\varrho}_i)\cdot d\mathbf{l}, \tag{4.2}$$

where

$$\boldsymbol{\alpha}(\mathbf{r} - \boldsymbol{\varrho}_i) = \mathbf{a}(\mathbf{r} - \boldsymbol{\varrho}_i) - \mathbf{a}'(\mathbf{r} - \boldsymbol{\varrho}_i). \tag{4.3}$$

The term $\mathbf{a}$, defined as

$$\mathbf{a}(\mathbf{r} - \boldsymbol{\varrho}_i) = a_{0\varphi}(\rho', z)\hat{\varphi}', \tag{4.4}$$

where

$$\rho' = [(x - x_i)^2 + (y - y_i)^2]^{1/2}$$

and

$$\hat{\varphi}' = [\hat{y}(x - x_i) - \hat{x}(y - y_i)]/\rho',$$

is just the vector potential produced in the space above the superconductor by a vortex line at $\boldsymbol{\varrho}_i$ and is given by Eq. (3.4) or by Eqs. (3.6) and (3.10) in the appropriate limits. The term $\mathbf{a}'$, defined as

$$\mathbf{a}'(\mathbf{r} - \boldsymbol{\varrho}_i) = (\varphi_0/2\pi\rho')\hat{\varphi}', \tag{4.5}$$

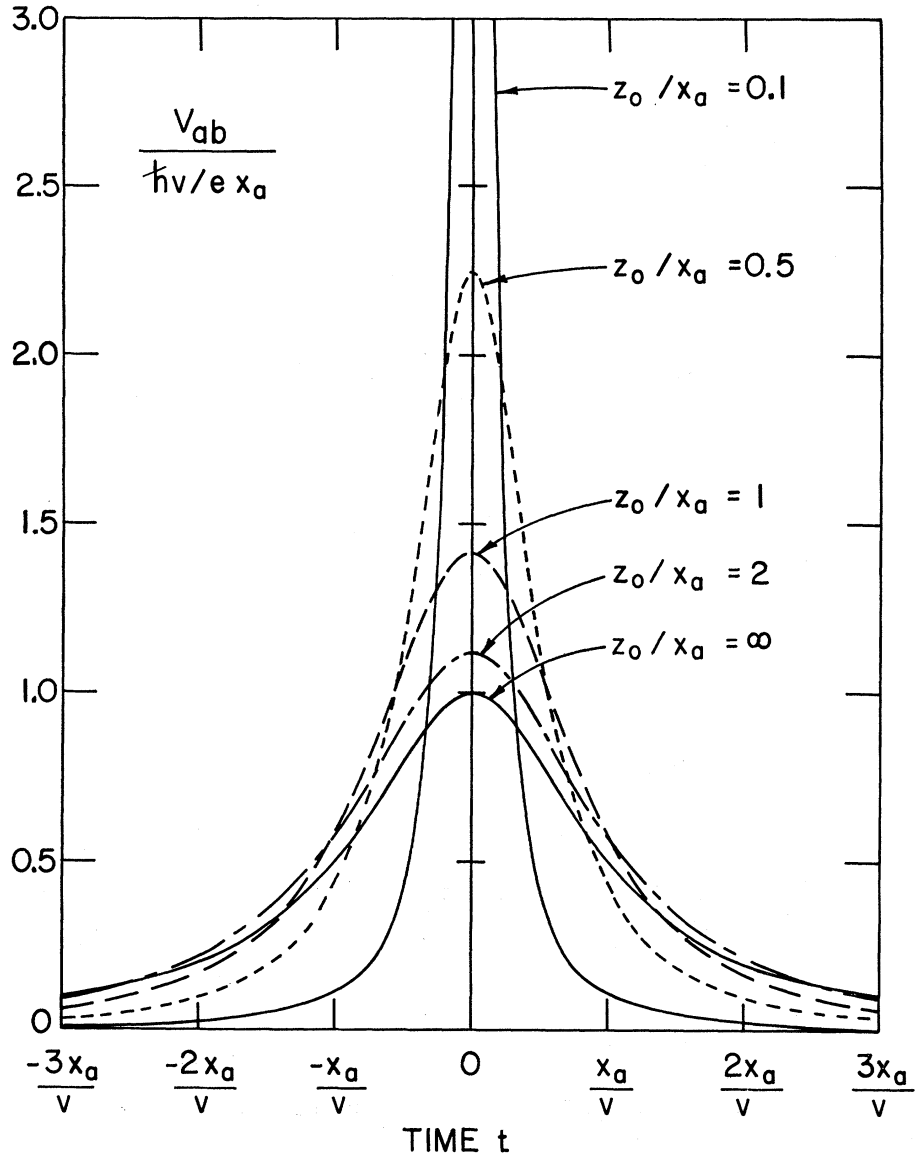

FIG. 4. Theoretical measured voltage pulse V_{ab} versus time t produced by the motion of a vortex line of coordinates $\mathbf{r}_i=(0,vt,0)$ through the circuit of Fig. 2 but with $x_b=-x_a$ and $y_a=y_b=0$, for various values of the ratio z_0/x_a. The area under each curve of V_{ab} versus t is $\varphi_0/c=h/2e$.

is chosen such that

$$\frac{1}{c}\frac{\partial}{\partial t}\int_{a[C_M]}^{b}\mathbf{a}'(\mathbf{r}-\boldsymbol{\varrho}_i)\cdot d\mathbf{l}=\psi(\mathbf{r}_a)-\psi(\mathbf{r}_b) \qquad (4.6)$$

gives the scalar potential difference between points a and b produced by a vortex at $\boldsymbol{\varrho}_i$ moving with velocity $\mathbf{v}_i$. The measured flux-flow voltage $V_{ab}(t)$, produced by a given distribution of vortices, is thus expressible as the sum of the individual contributions,

$$V_{ab}(t)=\sum_i V_{ab}{}^0(\boldsymbol{\varrho}_i,\mathbf{v}_i)=\sum_i \partial F_{ab}(\boldsymbol{\varrho}_i)/\partial t, \qquad (4.7)$$

where the sum extends over all vortices i in the superconductor.

We now wish to examine the dependence of $V_{ab}(t)$ upon the distribution of flux within the specimen. It is thus convenient to express the vortex density function in terms of a set of two-dimensional δ functions centered at the vortex positions,

$$n(\boldsymbol{\varrho},t)=\sum_i \delta^{(2)}(\boldsymbol{\varrho}-\boldsymbol{\varrho}_i(t)). \qquad (4.8)$$

The vortex current density,

$$\mathfrak{J}(\boldsymbol{\varrho},t)=\sum_i \dot{\boldsymbol{\varrho}}_i(t)\delta^{(2)}(\boldsymbol{\varrho}-\boldsymbol{\varrho}_i(t)), \qquad (4.9)$$

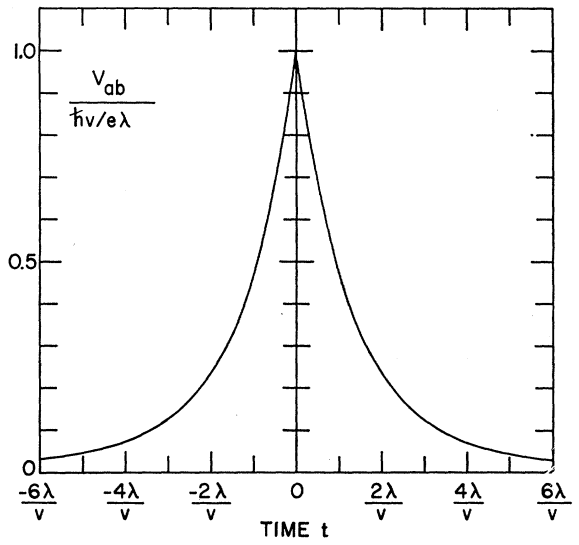

FIG. 5. Theoretical measured voltage pulse V_{ab} versus time t produced by the motion of a vortex line of coordinates $\mathbf{r}_i=(0,vt,0)$ through the circuit of Fig. 2, but with $x_b=-x_a$, $y_a=y_b=0$, and $z_0=0$. The area under the curve of V_{ab} versus t is $\varphi_0/c=h/2e$.

obeys the continuity equation describing conservation of flux lines,

$$\partial n(\boldsymbol{\varrho},t)/\partial t+\nabla\cdot\mathfrak{J}(\boldsymbol{\varrho},t)=0. \tag{4.10}$$

The time-dependent measured voltage may then be written in the following ways:

$$\begin{aligned}V_{ab}(t)&=\sum_i \partial F_{ab}(\boldsymbol{\varrho}_i)/\partial t=\sum_i \dot{\boldsymbol{\varrho}}_i\cdot\nabla F_{ab}(\boldsymbol{\varrho}_i)\\&=\int d^2\rho\mathfrak{J}(\boldsymbol{\varrho},t)\cdot\nabla F_{ab}(\boldsymbol{\varrho})\\&=\sum_\alpha\int d^2\rho\mathfrak{J}_\alpha(\boldsymbol{\varrho},t)\partial F_{ab}(\boldsymbol{\varrho})/\partial x_\alpha,\end{aligned} \tag{4.11}$$

where $\alpha=1(2)$ denotes the $x(y)$ component.

The time average $\bar{V}_{ab}$ of the measured voltage may be expressed in terms of the time-average vortex-current density $\langle\mathfrak{J}(\boldsymbol{\varrho})\rangle_t$:

$$\bar{V}_{ab}=\sum_\alpha\int d^2\rho\langle\mathfrak{J}_\alpha(\boldsymbol{\varrho})\rangle_t\partial F_{ab}(\boldsymbol{\varrho})/\partial x_\alpha. \tag{4.12}$$

(We shall henceforth denote space averages with brackets and time averages either with bars or with brackets and subscript t.)

The autocorrelation function,

$$\Psi(T)=\langle\delta V_{ab}(t)\delta V_{ab}(t+T)\rangle_t, \tag{4.13}$$

where $\delta V_{ab}(t)=V_{ab}(t)-\bar{V}_{ab}$, may be compactly expressed as

$$\Psi(T)=\sum_{\alpha\beta}\int d^2\rho\int d^2\rho' K_{\alpha\beta}(\boldsymbol{\varrho},\boldsymbol{\varrho}',T)[\partial F_{ab}(\boldsymbol{\varrho})/\partial x_\alpha]\times[\partial F_{ab}(\boldsymbol{\varrho}')/\partial x'_\beta], \tag{4.14}$$

where the vortex-current correlation function $K_{\alpha\beta}$, defined by

$$K_{\alpha\beta}(\boldsymbol{\varrho},\boldsymbol{\varrho}',T)=\langle[\mathfrak{J}_\alpha(\boldsymbol{\varrho},t)-\langle\mathfrak{J}_\alpha(\boldsymbol{\varrho})\rangle_t]\times[\mathfrak{J}_\beta(\boldsymbol{\varrho}',t+T)-\langle\mathfrak{J}_\beta(\boldsymbol{\varrho}')\rangle_t]\rangle_t, \tag{4.15}$$

contains information about the flux distribution, the transport current density, and the influence of pinning. The dependence of $\Psi(T)$ upon the measuring circuit configuration enters only through the terms in Eq. (4.14) involving F_{ab}.

The experimentally measured power spectrum $w(f)$ is derived from $\Psi(T)$ via the relation[11]

$$w(f)=4\int_0^\infty dT\,\Psi(T)\cos 2\pi fT. \tag{4.16}$$

We note that, by the inverse Fourier transform,

$$\Psi(T)=\int_0^\infty df\,w(f)\cos 2\pi fT. \tag{4.17}$$

The mean square noise voltage is related to $w(f)$ via

$$\langle\delta V_{ab}{}^2\rangle_t=\Psi(0)=\int_0^\infty df w(f). \tag{4.18}$$

B. Model Calculations

As shown above, the experimentally measured quantities $\bar{V}_{ab}$ and $w(f)$ may be calculated from the vortex current density $\mathfrak{J}(\boldsymbol{\varrho},t)$. However, such a calculation requires, in general, detailed knowledge of the transport current density distribution which drives the vortices, the distribution of pinning sites and their dynamical effects, and the vortex density distribution. In the following, we shall carry out a few model calculations which illustrate some of the main effects upon the experimental quantities.

1. Constant Vortex Velocities

We consider first the hypothetical case in which all vortices in the specimen move with constant velocity $\mathbf{v}=v\hat{\mathbf{y}}$ in the y direction. If $\bar{n}$ is independent of position, then

$$\mathfrak{J}(\boldsymbol{\varrho},t)=n(\boldsymbol{\varrho},t)\mathbf{v}, \tag{4.19}$$

$$\langle\mathfrak{J}\rangle_t=\bar{n}\mathbf{v}, \tag{4.20}$$

and

$$\bar{V}_{ab}=\bar{n}\varphi_0 v(x_a-x_b)/c. \tag{4.21}$$

[11] D. K. C. MacDonald, *Noise and Fluctuations* (John Wiley & Sons, Inc., New York, 1962), Chap. 2, p. 48.

We have used the result that $F_{ab}(x,y)$ has the value $F_{ab}(x,-\infty)=0$, and that it either attains the value $F_{ab}(x,\infty)=\varphi_0/c$ if the vortex passes between the voltage probe contacts ($x_b<x<x_a$) or else returns to the value $F_{ab}(x,\infty)=0$ if the vortex passes outside the contacts ($x<x_b$ or $x>x_a$).

The vortex-current correlation function in this case has the form

$$K_{\alpha\beta}=\delta_{\alpha 2}\delta_{\beta 2}v^2\langle[n(\varrho,t)-\bar{n}][n(\varrho',t+T)-\bar{n}]\rangle_t. \quad (4.22)$$

For the case of a liquidlike vortex line arrangement within the specimen, the density-density correlation function may be expressed, using procedures applicable to the electron gas,[12] in terms of a two-dimensional δ function describing the correlation of a vortex with itself and a radial distribution function $g(\varrho)$ describing its correlation with all the other vortices. Then

$$K_{\alpha\beta}(\varrho,\varrho',T)=K_{22}(\varrho-\varrho'+\mathbf{v}T)\delta_{\alpha 2}\delta_{\beta 2}, \quad (4.23)$$

where

$$K_{22}(\varrho)=\bar{n}v^2[\delta^{(2)}(\varrho)+\bar{n}g(\varrho)-\bar{n}]. \quad (4.24)$$

The radial distribution function is defined as

$$g(\varrho)=(\bar{n}N)^{-1}\sum_i\sum_{j\neq i}\delta^{(2)}(\varrho+\varrho_j-\varrho_i), \quad (4.25)$$

where the sums are taken over the N vortices in the specimen. (We shall be interested, however, only in the limit $N\to\infty$.) The quantity $\bar{n}g(\varrho)$ is the average density of vortices per unit area at a point ϱ when a vortex is known to be located at the point $\varrho=0$. As $\rho\to 0$, $g(\varrho)\to 0$, since vortices repel each other at close range, and as $\rho\to\infty$, $g(\varrho)\to 1$, since there is no correlation between vortex positions at large separations.

Upon introducing a change of variables we note that the autocorrelation function may be written as

$$\Psi(T)=\bar{n}v^2\int d^2\rho[\delta^{(2)}(\varrho)+\bar{n}g(\varrho)-\bar{n}]G(\varrho-\mathbf{v}T), \quad (4.26)$$

where

$$G(\varrho)=\int d^2\rho'[\partial F_{ab}(\varrho'+\varrho)/\partial y'][\partial F_{ab}(\varrho')/\partial y'] \quad (4.27)$$

contains all the information concerning the spatial configuration of the measuring circuit. The function $G(\varrho)$ is large only in the region between and near the voltage probe contacts, is typically a slowly varying function of ϱ by comparison with $g(\varrho)$, and decreases rapidly as ρ exceeds a length of the order of the voltage probe contact separation. Using the same argument as that leading to Eq. (4.21), we find that

$$\int d^2\rho G(\varrho)=[\varphi_0(x_a-x_b)/c]^2. \quad (4.28)$$

In the event of no correlation between vortex positions the radial distribution $g(\varrho)$ has the value unity in the limit $N\to\infty$, and the autocorrelation function becomes

$$\Psi(T)=\bar{n}v^2G(-\mathbf{v}T). \quad (4.29)$$

Since G also obeys

$$\int_0^\infty dTG(-vT)=(\varphi_0/c)^2(x_a-x_b)/2v, \quad (4.30)$$

the corresponding power spectrum $w(f)$, given by Eq. (4.16), obeys, in the limit $f\to 0$,

$$w(0)=2\bar{n}v(\varphi_0/c)^2(x_a-x_b)=2\bar{V}_{ab}\varphi_0/c. \quad (4.31)$$

To be more realistic, however, we should take into account the short-range correlation between vortex positions. Let us assume that $g(\varrho)$ has an appropriate spatial variation out to some characteristic range of correlation ρ_c, beyond which $g(\varrho)=g_\infty$, a constant. A measure of the correlation between vortex positions is the integral

$$\int d^2\rho[\bar{n}g(\varrho)-\bar{n}]=N_c, \quad \rho<\rho_c \quad (4.32)$$

where we interpret N_c as the number of vortices whose positions are correlated with the position of a given vortex. This number would be large, for example, if vortices tended to travel in "clumps" or "bundles" of high vortex density. If the range ρ_c is small by comparison with the range of $G(\varrho)$, then, since $g_\infty\to 1$ in the limit $N\to\infty$, the autocorrelation function becomes

$$\Psi(T)=(1+N_c)\bar{n}v^2G(-\mathbf{v}T). \quad (4.33)$$

The corresponding power spectrum $w(f)$ obeys, in the limit $f\to 0$,

$$w(0)=(1+N_c)(2\bar{V}_{ab}\varphi_0/c). \quad (4.34)$$

We note that the magnitudes of this autocorrelation function and the power spectrum are larger by a factor of $1+N_c$ than those in the uncorrelated case, Eqs. (4.29) and (4.31). A similar enhancement factor was required in the interpretation of van Gurp's experimental results,[2] in which this factor was regarded as the number of fluxoids in a flux bundle.

As an explicit example of the power spectrum resulting from Eqs. (4.33) and (4.34) for a given measuring circuit configuration, the theoretical result for the experimental configuration of Fig. 2 with $z_0=\infty$ is

$$w(f)=w(0)\{\tfrac{1}{2}\exp(-2\pi f/f_x)\cos(2\pi f/f_y) +\tfrac{1}{2}(f_x/2\pi f)[1-\exp(-2\pi f/f_x)\cos(2\pi f/f_y)]\}. \quad (4.35)$$

The details of this calculation are left to Appendix A. The shape of the power spectrum is determined only by the characteristic lengths of the measuring circuit, $|x_{ab}|=|x_a-x_b|$ and $|y_{ab}|=|y_a-y_b|$, and the speed v of the vortex motion, which together fix the characteristic frequencies $f_x=v/|x_{ab}|$ and $f_y=v/|y_{ab}|$. The

[12] D. Pines, *Elementary Excitations in Solids* (W. A. Benjamin, Inc., New York, 1963), Chap. 3, p. 72.

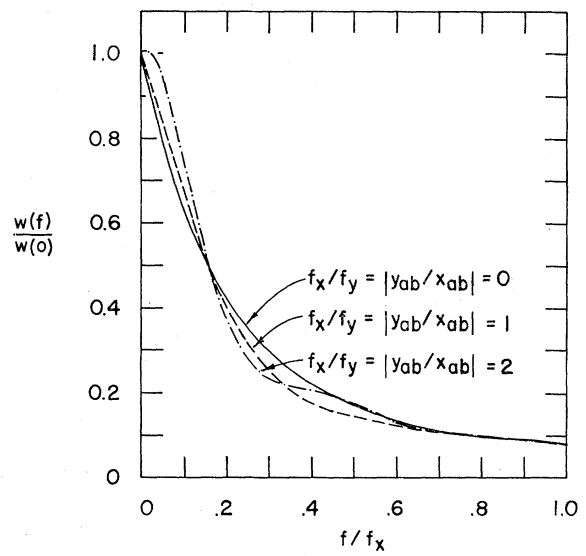

FIG. 6. Theoretical reduced power spectrum $w(f)/w(0)$ versus reduced frequency f/f_x, where $f_x=v/|x_a-x_b|$, for the measuring circuit of Fig. 2 with $z_0=\infty$ and for the model described in the text of vortex motion with constant speed v in the y direction. The dependence upon the circuit geometry is shown for several values of $f_x/f_y=|y_a-y_b|/|x_a-x_b|$.

reduced power spectrum $w(f)/w(0)$ is plotted versus f/f_x for several values of $f_x/f_y=|y_{ab}|/|x_{ab}|$ in Fig. 6. An interesting feature of this power spectrum is the behavior $w(f)\propto f^{-1}$ as $f\to\infty$, arising physically from the sharply peaked voltage pulses produced by vortices passing very close to the voltage probe contacts, here assumed infinitesimal in size. This leads to a logarithmic divergence in the mean square noise voltage $\langle\delta V_{ab}^2\rangle=\Psi(0)$. In a realistic situation the power spectrum will decay more rapidly than f^{-1} for frequencies above $f_{\max}\sim v/L_{\max}$, where $L_{\max}$ is the larger of the radius of the probe contact or the vortex core radius.

2. *Noise Reduction with Long-Range Correlation*

For the case that the range of correlation ρ_c of the intervortex separation is large by comparison with a typical measuring circuit dimension, as in the case of a nearly perfect vortex lattice, there should be a great reduction in the noise voltage. A simple argument, though involving some rough approximations, may be helpful to demonstrate this effect: Each vortex which passes between the voltage-probe contacts produces a voltage pulse whose time integral is φ_0/c. Since the width of the pulse in time is of order L/v, where L is a typical circuit dimension and v is the vortex speed, a vortex makes a contribution to the measured voltage of order $v\varphi_0/cL$ when it is in the vicinity of the contacts. The voltage measured at a given time is of order $V_{ab}(t)\sim N'v\varphi_0/cL$, where $N'\sim\bar{n}L^2$ is the number of contributing vortices between and near the probe contact sat this time. The time-average voltage is thus of order $\bar{V}_{ab}\sim\bar{n}\varphi_0Lv/c$. If the positions of vortices are uncorrelated, then the number N' of contributing vortices fluctuates statistically with time with excursions of order $(\bar{N}')^{1/2}\sim\bar{n}^{1/2}L$ from the average value $\bar{N}'\sim\bar{n}L^2$. This produces a fluctuating component δV_{ab} of the measured voltage and a mean square noise voltage of order $\langle\delta V_{ab}^2\rangle_t\sim\bar{n}(v\varphi_0/c)^2\sim\bar{V}_{ab}(v\varphi_0/cL)$.

However, if there is a high degree of correlation between vortex positions over a range ρ_c large by comparison with L, the number of contributing vortices N' and, hence, the measured voltage $V_{ab}(t)\sim N'v\varphi_0/cL$ are maintained essentially constant over times of order ρ_c/v, large by comparison with L/v. This results in a low-noise situation in which the magnitudes of the fluctuating component of the measured voltage, the mean square voltage, and the power spectrum are reduced from those in the uncorrelated case.

It would be interesting to see whether such a state of long-range correlation, as in the case of a nearly perfect vortex lattice, could be produced experimentally during flux-flow measurements. Perhaps this could be accomplished at fields near H_{c2} when the vortex lattice presumably becomes very rigid. The chief experimental evidence for such a state would be a significant change in the shape of the power spectrum from that calculated using Eq. (4.33) for the case of short-range correlation. If the range of correlation ρ_c were much larger than a typical circuit dimension L, then the autocorrelation function $\Psi(T)$ would vary on a time scale given by ρ_c/v rather than L/v and the power spectrum $w(f)$ would vary on a frequency scale given by v/ρ_c rather than v/L. Moreover, the shape of the power spectrum versus frequency would be independent of the spatial configuration of the voltmeter leads above the surface of the superconductor. If ρ_c does become infinite at H_{c2}, this would lead to the intuitively pleasing situation in which the power spectrum in the mixed state changes shape as the applied field is increased and goes over continuously to the normal state value, essentially zero, at H_{c2}.

3. *Pinning Effects*

We now consider some effects of an inhomogeneous distribution of pinning centers upon a set of uncorrelated vortices. As a model to compute these effects we shall assume that all vortices move in the y direction but with a speed determined by the local pinning forces. It is convenient to introduce a function $Y(x_i, t-t_i)$ which specifies the y coordinate of a vortex i of x coordinate x_i which crosses the x axis at time t_i. Then the vortex position $\boldsymbol{\varrho}_i(t)=(x_i,y_i(t))$ is given by

$$y_i(t)=Y(x_i, t-t_i). \tag{4.36}$$

We note that $y_i(t_i)=0$ by definition. The vortex density distribution is then

$$n(\boldsymbol{\varrho},t)=\sum_i \delta(x-x_i)\delta(y-Y(x_i, t-t_i)), \tag{4.37}$$

and the vortex current is $\mathfrak{J}=\mathfrak{J}\hat{y}$ where

$$\mathfrak{J}(\varrho,t)=\sum_i \dot{Y}(x_i, t-t_i)\delta(x-x_i) \times\delta(y-Y(x_i, t-t_i)). \quad (4.38)$$

The time average of the vortex current is now easily computed by replacing the sum over vortex positions by an integral

$$\sum_i = \int dx_i \int dt_i \langle n\rangle \bar{v}(x_i), \quad (4.39)$$

where $\langle n\rangle$ is the space-average density of vortices per current area of the specimen and $\bar{v}(x_i)$ is the time-averaged speed of a vortex as it moves along the plane $x=x_i$. Thus,

$$\langle \mathfrak{J}(x)\rangle_t = \langle n\rangle \bar{v}(x). \quad (4.40)$$

The measured voltage $V_{ab}(t)$ is given by

$$V_{ab}(t) = \int d^2\rho \mathfrak{J}(\varrho,t)\partial F_{ab}(\varrho)/\partial y, \quad (4.41)$$

and its time average is

$$\bar{V}_{ab} = (\langle n\rangle \varphi_0/c) \int_{x_b}^{x_a} dx \bar{v}(x). \quad (4.42)$$

The calculation of the vortex-current correlation function, including only the correlation of a given vortex with itself, may be expressed in terms of a sum on i. The time average may again be carried out by the replacement of this sum by the integral as in Eq. (4.39) with the result that

$$K_{\alpha\beta} = K_{22}\delta_{\alpha 2}\delta_{\beta 2}, \quad (4.43)$$

where

$$K_{22}(\varrho,\varrho',T) = \langle n\rangle \bar{v}(x)\delta(x-x') \int dt \dot{Y}(x,t)\delta(y-Y(x,t)) \times \dot{Y}(x, t+T)\delta(y'-Y(x, t+T)). \quad (4.44)$$

For the case that $Y(x,t)=\bar{v}(x)t$, we have

$$K_{22}(\varrho,\varrho,T) = \langle n\rangle \bar{v}^2(x)\delta(x-x')\delta(y-y'+\bar{v}(x)T). \quad (4.45)$$

The corresponding autocorrelation function is

$$\Psi(T) = \int d^2\rho \langle n\rangle \bar{v}^2(x)[\partial F_{ab}(x,y)/\partial y] \times[\partial F_{ab}(x, y+\bar{v}(x)T)/\partial y]. \quad (4.46)$$

Although the power spectrum $w(f)$ obeys, in the limit as $f\to 0$,

$$w(0) = (2\bar{V}_{ab}\varphi_0/c), \quad (4.47)$$

the same value as in the case of a constant vortex speed, the shape of the power spectrum is altered from that appropriate for a constant speed. We may regard this as arising from a spectrum of characteristic frequencies determined by the spatial variation of $\bar{v}(x)$ over the specimen.

For the case that $\dot{Y}(x,t)$ is not independent of time but varies on a time scale set by $L_p/\bar{v}$ where L_p is the characteristic distance between pinning sites, the autocorrelation function $\Psi(t)$ has superimposed upon it an oscillatory structure of period $L_p/\bar{v}$. The corresponding power spectrum still obeys Eq. (4.47) in the limit as $f\to 0$, but possesses additional structure at a frequency of the order of $\bar{v}/L_p$. However, if L_p is small by comparison with typical circuit dimensions, then this frequency is relatively large and the corresponding structure is not observed if one examines only the frequency range from zero to $\bar{v}/(x_a-x_b)$. Moreover, at these low frequencies, the power spectrum may be calculated to good approximation with the use of the autocorrelation function $\Psi(T)$ of Eq. (4.46) in which only the time-averaged value $\bar{v}(x)$ appears.

The effect of short-range correlation between vortex positions may evidently be taken into account, if only crudely, by the inclusion of the factor $1+N_c$ on the right-hand side of Eq. (4.46). The quantity N_c, a measure of the correlation of vortex positions, must be defined in a fashion similar to that of Eq. (4.32). The value of $w(f)$ in the limit as $f\to 0$ thus becomes

$$w(0) = (1+N_c)(2\bar{V}_{ab}\varphi_0/c). \quad (4.48)$$

Experimental studies of the power spectrum at high frequencies and low current densities may, as discussed above, yield information about the characteristic distance between pinning sites. However, such studies could be complicated by a similar phenomenon which van Gurp calls flicker noise.[2] This noise, which occurs only above the helium λ point, arises from time-varying vortex velocities associated with local temperature variations produced by helium-bubble formation.

4. *Flux-Line Dislocation Dipoles*

Kramer[13] has shown that under certain conditions flux transport is best described in terms of the motion of flux-line dislocation (FLD) dipoles. Since this description is likely to be an increasingly important key to the understanding of flux motion and flux pinning, it is useful to see how the above treatment of the noise voltage can be used to account for FLD-dipole motion.

We consider a semi-infinite superconductor in the half-space $z<0$ containing vortex lines parallel to the z axis. We suppose that the vortices form a perfect triangular lattice except in the vicinity of two edge dislocations of opposite sign, a dipole, sketched in Fig. 7. These dislocations are parallel to the z axis, with both sense vectors $\hat{\xi}$ in the z direction, and intersect the plane $z=0$ at time $t=0$ at the points $\varrho_-=(-\frac{1}{2}x_s, -\frac{1}{2}y_s)$ and $\varrho_+=(\frac{1}{2}x_s, \frac{1}{2}y_s)$. The Burgers vectors are for ϱ_-, $\mathbf{b}_-=-b\hat{y}$, and for ϱ_+, $\mathbf{b}_+=b\hat{y}$. The length b of the

[13] E. J. Kramer, J. Appl. Phys. (to be published).

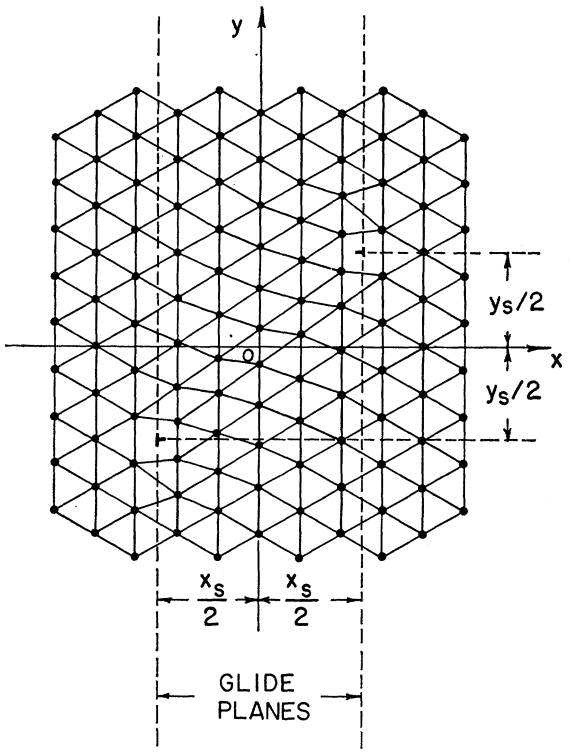

FIG. 7. Schematic view of a dipole of edge dislocations, indicated by the symbol $\perp$, of glide plane separation x_s in an otherwise perfect triangular vortex lattice.

Burgers vector is equal to the intervortex spacing. Thus $b^2=2/\langle n\rangle\sqrt{3}$, where $\langle n\rangle$ is the space-averaged density of vortices per unit area. The edge dislocations are assumed unable to climb and able only to glide in the parallel glide planes $x=-\frac{1}{2}x_s$ and $x=\frac{1}{2}x_s$. From consideration of the interaction energy between the dislocations, such a dipole is found to achieve a stable equilibrium only when $y_s=x_s$.[14]

If the dipole moves with constant velocity $\mathbf{v}_d=v_d\hat{y}$ in the y direction, scalar and vector potentials are generated by the collective motion of vortices in the vicinity of the dipole. As shown in Appendix B, the measured voltage V_{ab} produced by a dipole which is at the origin at time $t=0$ is given to good approximation by

$$V_{ab}\approx\langle n\rangle bx_s\partial F_{ab}(\mathbf{v}_d t)/\partial t. \tag{4.49}$$

As seen by comparison with Eq. (4.1), the resulting measured voltage appears as if it were produced by a bundle of $\langle n\rangle bx_s$ flux quanta at the site of the dipole moving with the dipole velocity $\mathbf{v}_d$.

We now consider an array of such dipoles whose centers intersect the plane $z=0$ at time t at the coordinates $\mathbf{r}_i=\boldsymbol{\varrho}_i=(x_i,y_i,0)$. The dipole density function,

$$n_d(\boldsymbol{\varrho},t)=\sum_i \delta^{(2)}(\boldsymbol{\varrho}-\boldsymbol{\varrho}_i(t)), \tag{4.50}$$

where the sum extends over all dipoles, specifies the number of FLD dipoles per unit area. The dipole current density is given by

$$\mathfrak{J}_d(\boldsymbol{\varrho},t)=n_d(\boldsymbol{\varrho},t)\mathbf{v}_d. \tag{4.51}$$

Since each dipole transports $\langle n\rangle bx_s$ flux quanta, the vortex current density is given approximately by

$$\mathfrak{J}(\boldsymbol{\varrho},t)=\langle n\rangle bx_s\mathfrak{J}_d(\boldsymbol{\varrho},t)=\langle n\rangle bx_s n_d(\boldsymbol{\varrho},t)\mathbf{v}_d, \tag{4.52}$$

and its time average is given by

$$\langle\mathfrak{J}\rangle_t=\langle n\rangle bx_s\langle n_d\rangle\mathbf{v}_d. \tag{4.53}$$

Thus, the time-averaged measured voltage is

$$\bar{V}_{ab}=\langle n\rangle bx_s\langle n_d\rangle\varphi_0 v_d(x_a-x_b)/c. \tag{4.54}$$

For the case of a liquidlike arrangement of dipoles within the specimen the vortex-current correlation function has the form

$$K_{\alpha\beta}(\boldsymbol{\varrho},\boldsymbol{\varrho}',T)=K_{22}(\boldsymbol{\varrho}-\boldsymbol{\varrho}'+\mathbf{v}_d T)\delta_{\alpha 2}\delta_{\beta 2}, \tag{4.55}$$

where

$$K_{22}(\boldsymbol{\varrho})=(\langle n\rangle bx_s)^2 v_d^2\bar{n}_d[\delta^{(2)}(\boldsymbol{\varrho})+\bar{n}_d g_d(\boldsymbol{\varrho})-\bar{n}_d]. \tag{4.56}$$

The dipole radial distribution function g_d is defined as

$$g_d(\boldsymbol{\varrho})=(\bar{n}_d N_d)^{-1}\sum_i\sum_{j\neq i}\delta^{(2)}(\boldsymbol{\varrho}+\boldsymbol{\varrho}_j-\boldsymbol{\varrho}_i), \tag{4.57}$$

where the sums are taken over the N_d dipoles in the specimen.

In the case of no correlation between dipole positions we obtain the analog of Eq. (4.29),

$$\Psi(T)=\bar{n}_d(\langle n\rangle bx_s)^2 v_d^2 G(-\mathbf{v}_d T). \tag{4.58}$$

The corresponding power spectrum, given by Eq. (4.16), obeys, in the limit $f\to 0$,

$$w(0)=(\langle n\rangle bx_s)(2\bar{V}_{ab}\varphi_0/c). \tag{4.59}$$

If there is correlation between dipole positions characterized by a range ρ_d, as would be the case if dipoles tended to travel in groups as suggested by Kramer,[13] then a measure of this correlation is the integral corresponding to Eq. (4.32),

$$\int d^2\rho[\bar{n}_d g_d(\mathbf{p})-\bar{n}_d]=N_{cd},\quad \rho<\rho_d. \tag{4.60}$$

We interpret N_{cd} as the number of FLD dipoles whose positions are correlated with the position of a given dipole. If ρ_d is small by comparison with the range of $G(\boldsymbol{\varrho})$, then the autocorrelation function is given by Eq. (4.58), multiplied by $(1+N_{cd})$. The corresponding power spectrum obeys, in the limit $f\to 0$,

$$w(0)=(1+N_{cd})(\langle n\rangle bx_s)(2\bar{V}_{ab}\varphi_0/c). \tag{4.61}$$

The prefactor $(1+N_{cd})(\langle n\rangle bx_s)$ plays the role of the number of flux quanta in a flux bundle as defined operationally by van Gurp.[2]

[14] F. R. N. Nabarro, Advan. Phys. 1, 271 (1952).

If the range of correlation ρ_d is large by comparison with typical circuit dimensions, there should be a significant reduction in the noise voltage and in the value of $w(f)$, as discussed earlier.

The influence of an inhomogeneous distribution of dipole pinning centers upon a set of identical FLD dipoles can be estimated with a model similar to that leading to Eqs. (4.42)–(4.48). The results may be expressed in terms of the time-averaged dipole velocity $\bar{v}_d(x)$, for dipoles moving in the y direction with x coordinate x, and the correlation factor N_{cd} of Eq. (4.60). The time-averaged measured voltage is

$$\bar{V}_{ab}=(\langle n\rangle bx_s\langle n_d\rangle\varphi_0/c)\int_{x_b}^{x_a}dx\bar{v}_d(x)\,, \qquad (4.62)$$

where $\langle n_d\rangle$ is the space-average density of dipoles per unit area. For short-range correlation the power spectrum obeys Eq. (4.61) in the limit $f\rightarrow 0$. If the typical distance between dipole pinning centers L_{pd} is small by comparison with a characteristic circuit dimension L, then the power spectrum should exhibit structure at high frequencies of order $\bar{v}_d/L_{pd}$. However, at low frequencies of order $\bar{v}_d/L$ and below, the power spectrum may be calculated to good approximation from

$$\Psi(T)\approx(1+N_{cd})(\langle n\rangle bx_s)^2\langle n_d\rangle\int d^2\rho[\bar{v}_d(x)]^2$$

$$\times[\partial F_{ab}(x,y)/\partial y][\partial F_{ab}(x,\,y+\bar{v}_d(x)T)/\partial y]. \qquad (4.63)$$

Evidently, long-range correlation and the accompanying noise reduction can occur only near H_{c2}. However, at this field pinning effects are relatively unimportant.

C. Discussion of Previous Experiments

The effective bundle size, using the name given by by van Gurp[2] to define the quantity

$$N_b=w(0)/(2\bar{V}_{ab}\varphi_0/c)\,, \qquad (4.64)$$

has the following values under the conditions described above:

(1) $N_b=(1+N_{cd})\langle n\rangle bx_s$, for motion of flux-line dislocation dipoles of Burgers vector b and glide plane separation x_s with short-range correlation,

(2) $N_b=\langle n\rangle bx_s$, for uncorrelated motion of FLD dipoles,

(3) $N_b=(1+N_c)$, for motion of individual vortices with short-range correlation,

(4) $N_b=1$, for uncorrelated motion of indivudal vortices, and

(5) $N_b\ll 1$, for long-range correlation.

In van Gurp's experiments,[2] the value of N_b was observed to be very large (10^3–10^5) at low applied field, low temperature, and low transport current density, but to decrease towards unity as the field, temperature, and current density increased. The present analysis thus lends support to Kramer's[13] conjecture that, at low values of the applied magnetic field and the transport current density, flux flow is characterized by the correlated motion of FLD dipoles. At higher values, presumably N_{cd} and $\langle n\rangle bx_s$ would decrease, reducing the value of N_b. As the applied field approaches H_{c2} and at high current densities, the FLD dipole density evidently becomes very large and the flux distribution is probably better described in terms of correlated motion of individual vortices. Near H_{c2}, where van Gurp found $N_b\approx 1$, the noise spectrum seems to be characterized by the motion of individual vortices in an essentially uncorrelated, fluidlike distribution.

A puzzling feature of van Gurp's experiments[2] is that $w(f)$ was observed to exhibit a maximum at a low frequency and a sharp decrease at still lower frequencies. This behavior implies structure in the autocorrelation function $\Psi(T)$ at times T large by comparison with the time taken for vortices to traverse the measuring circuit. However, such behavior is not found for the simple flux distribution models considered above. Perhaps some sort of time-dependent, long-range correlation of the flux distribution is responsible for this effect. The physical origin of the low-frequency maximum in $w(f)$ remains, we feel, an open question and warrants additional experimental and theoretical investigation.

So far we have seen that by examining the zero frequency limit of $w(f)$ a physically interesting quantity, the bundle size N_b, may be obtained. Another important piece of information bearing upon the validity of the FLD dipole description should be obtainable from an examination of the frequency dependence of $w(f)$. We consider the dimensionless parameter

$$R=c\bar{V}_{ab}/Bf_cL_1L_2\,, \qquad (4.65)$$

where B is the average magnetic induction threading the specimen, L_1 and L_2 are appropriate measuring circuit dimensions, and f_c is a frequency, characteristic of the low-frequency behavior of $w(f)$, suitably chosen such that: (1) $R=1$, for the uniform motion of individual vortices, and (2) $R=\langle n_d\rangle bx_s$, for the uniform motion of FLD dipoles of space-averaged density $\langle n_d\rangle$.

As an example, we consider the uniform motion of either individual vortices of velocity $\mathbf{v}=v\hat{y}$ or of FLD dipoles of velocity $\mathbf{v}_d=v_d\hat{y}$ through the measuring circuit of Fig. 2 with $z_0=\infty$ and $y_a=y_b$. The appropriate measuring circuit lengths for this circuit are $L_1=L_2=|x_a-x_b|$. If the flux flow is described by the motion of individual vortices, then $f_c=v/|x_a-x_b|$, and from Eqs. (4.21) and (4.65) we obtain $R=1$. However, if the flux flow is described by the motion of well-separated ($\langle n_d\rangle x_s^2\ll 1$) FLD dipoles, then $f_c=v_d/|x_a-x_b|$, and from Eqs. (4.54) and (4.65) we obtain $R=\langle n_d\rangle bx_s\ll 1$. It should thus be easy to determine experimentally which of the two flux-flow descriptions is appropriate.

Applying this analysis to van Gurp's experimental results,[2] we find additional support for the FLD dipole description at low transport current density. For the interpretation of his experiments, van Gurp found it necessary to introduce an empirical quantity p which he called the pinned fraction of vortices. From Eqs. (3) and (9) of Ref. 2, we note that $1-p$ plays the role of R defined by Eq. (4.65) above and may be regarded in the present context as the fraction of vortices $\langle n_d\rangle bx_s$ which are effectively transported at the FLD dipole speed v_d. With this interpretation, van Gurp's experimental results indicate that, for the specimens studied, $R=(1-p)=\langle n_d\rangle bx_s$ was considerably less than unity at low transport current density, implying low FLD dipole density, and that R increased at higher currents, implying increased dipole density.

V. TYPE-I SUPERCONDUCTORS

As was shown by Solomon,[15] the behavior of type-I superconducting strips in the intermediate state is in many respects similar to that of type-II superconducting strips in the mixed state. At low applied transverse fields, flux enters the type-I strips in the form of normal domains containing flux $\Phi\gg\varphi_0$, which move under the influence of an applied current and produce a flux-flow voltage. At high fields the normal regions coalesce into immobile domains which align themselves across the specimen perpendicular to the applied current. The current then flows through rigid normal domains, resulting in an Ohmic voltage drop across the specimen. Thus, the measured voltage arises from flux flow at low fields and from Ohmic resistance at high fields.

In the low-field case the time-dependent flux-flow voltage and its corresponding power spectrum may be calculated by methods similar to those used in the previous sections, except that the flux unit φ_0 must be replaced by Φ. As in Sec. III, the scalar potential Ψ generated by the flux motion may be regarded as arising from a motion-induced charge density on the boundaries of the moving normal domains. The measured voltage $V_{ab}(t)$ may be expressed in terms of $V_{ab}{}^S(t)$ and $V_{ab}{}^M(t)$, which have the same qualitative properties as discussed in Secs. III and IV. The power spectrum calculations of Sec. IV thus apply to the intermediate state, provided φ_0 is replaced by Φ. For example, in the case of the motion of a liquidlike distribution of uncorrelated normal domains, the power spectrum $w(f)$ has the value $w(0)=2\bar{V}_{ab}\Phi/c$ in the limit $f\to 0$.

Park's conjectures[16] that the potential term $V_{ab}{}^S$ obeys $V_{ab}{}^S=0$ in the intermediate state of type-I superconductors and that $V_{ab}{}^S\ll\bar{V}_{ab}$ in the mixed state of type-II superconductors near the lower critical field are not supported by the present model, nor is his conjecture that the time-varying components of the measured voltage arise entirely from fluctuations in $V_{ab}{}^M$. In the present model $\bar{V}_{ab}=\bar{V}_{ab}{}^S$ in both the intermediate and the mixed state. Moreover, Park's claims that the decrease in noise in the mixed state observed with increasing applied magnetic field corresponds to the decrease in the ratio $V_{ab}{}^M/\bar{V}_{ab}$ and that the noise decrease has nothing to do with a decrease in size of the flux entities with increasing field are not justified in light of the present calculations.

VI. DISCUSSION

The above model calculations provide a useful description of measured time-dependent flux-flow voltages. Perhaps the chief asset of the calculation of Sec. III is that the potentials, fields, and measured voltage produced by a moving fluxoid can be expressed in a simple analytic form. An interesting result is that the time integral of V_{ab} over the history of a single fluxon yields a contribution of magnitude $\varphi_0/c=h/2e$ if the fluxon passes between the voltage probe contacts and zero contribution otherwise. Of interest also is the result that voltage pulse shapes are easily calculable and are seen to depend upon the spatial configuration of the measuring circuit leads. That the pulse shapes also depend upon the specimen shape will be shown in a subsequent paper.

That the distribution of flux within the specimen and the modes of flux motion strongly affect the measured power spectrum is nicely demonstrated by the present model. These calculations also suggest experimental methods to determine whether flux flow in type-II superconductors at low fields and current densities may be best described in terms of flux-line dislocation dipoles.

A number of experimental checks on the present theory would be desirable:

(1) Power spectra could be studied using well-behaved specimens approximating the geometry of Sec. III by attaching voltage probe contacts on the center of a flat specimen whose dimensions were large by comparison with the probe separation. The shapes of the power spectra versus frequency could be compared with those calculated for a variety of configurations of the leads above the surface.

(2) The predicted dependence upon the probe contact dimensions could be tested.

(3) Power spectra for thin slabs could be compared with those which may be calculated for small and large ratios of the probe separation to the specimen width.

(4) Once the characteristic shape of the power spectrum for a specific circuit configuration and specimen shape is well understood, the behavior as a function of sample preparation, applied magnetic field, tempera-

[15] P. R. Solomon, Phys. Rev. **179**, 475 (1969).
[16] J. G. Park, J. Phys. **C2**, 742 (1969).

ture, and transport current density could be studied and related to pinning effects, flux distribution, and modes of flux motion.

The present theoretical description provides, we feel, a basic framework for the interpretation of experimental studies of time-dependent flux-flow noise voltages and their corresponding power spectra. Such experiments show promise of yielding important information about the nature of flux flow and pinning effects.

ACKNOWLEDGMENTS

The author is pleased to acknowledge stimulating discussions with Dr. G. J. van Gurp, Dr. J. Lowell, Dr. J. G. Park, and Dr. C. H. Weijsenfeld.

APPENDIX A

For the measuring circuit configuration of Fig. 2 with $z_0=\infty$, the functions F_{ab} and G, obtained from Eqs. (4.2) and (4.27), have the following properties:

$$F_{ab}(x,y)=\left(\frac{\varphi_0}{2\pi c}\right)\left(\tan^{-1}\frac{y_b-y}{x_b-x}-\tan^{-1}\frac{y_a-y}{x_a-x}\right), \tag{A1}$$

$$\frac{\partial F_{ab}(x,y)}{\partial y}=\left(\frac{\varphi_0}{2\pi c}\right)\left(\frac{(x_a-x)}{(x_a-x)^2+(y_a-y)^2}-\frac{(x_b-x)}{(x_b-x)^2+(y_b-y)^2}\right), \tag{A2}$$

$$G(x,y)=\pi\left(\frac{\varphi_0}{2\pi c}\right)^2\left[\frac{2y^2}{x^2+y^2}-\frac{(y-y_{ab})^2}{(x-x_{ab})^2+(y-y_{ab})^2}-\frac{(y+y_{ab})^2}{(x+x_{ab})^2+(y+y_{ab})^2}+\tfrac{1}{2}\ln\left(\frac{[(x-x_{ab})^2+(y-y_{ab})^2][(x+x_{ab})^2+(y+y_{ab})^2]}{(x^2+y^2)^2}\right)\right], \tag{A3}$$

where $x_{ab}=x_a-x_b$ and $y_{ab}=y_a-y_b$. The autocorrelation function $\Psi(T)$, obtained from Eq. (4.33), is given by

$$\Psi(T)=(1+N_c)\bar{n}v^2G(0,-vT). \tag{A4}$$

The resulting power spectrum $w(f)$ given by Eqs. (4.34) and (4.35) is obtained by carrying out the integration prescribed in Eq. (4.16).

APPENDIX B

The displacement field $\mathbf{u}(x,y,t)$ at time t for a vortex lattice subject to the edge dislocation dipole defined in Sec. IV B and sketched in Fig. 7 may be obtained from expressions derived by Nabarro.[14] The x and y components of this field at time $t=0$ are

$$u_x(x,y,0)=-\frac{(1-2\sigma)b}{8\pi(1-\sigma)}\ln\left(\frac{(x+\frac{1}{2}x_s)^2+(y+\frac{1}{2}y_s)^2}{(x-\frac{1}{2}x_s)^2+(y-\frac{1}{2}y_s)^2}\right)+\frac{b}{4\pi(1-\sigma)}\left(\frac{(x+\frac{1}{2}x_s)^2}{(x+\frac{1}{2}x_s)^2+(y+\frac{1}{2}y_s)^2}-\frac{(x-\frac{1}{2}x_s)^2}{(x-\frac{1}{2}x_s)^2+(y-\frac{1}{2}y_s)^2}\right), \tag{B1}$$

$$u_y(x,y,0)=\frac{b}{4\pi(1-\sigma)}\left(\frac{(x+\frac{1}{2}x_s)(y+\frac{1}{2}y_s)}{(x+\frac{1}{2}x_s)^2+(y+\frac{1}{2}y_s)^2}-\frac{(x-\frac{1}{2}x_s)(y-\frac{1}{2}y_s)}{(x-\frac{1}{2}x_s)^2+(y-\frac{1}{2}y_s)^2}\right)-\frac{b}{2\pi}\left(\tan^{-1}\frac{y+\frac{1}{2}y_s}{x+\frac{1}{2}x_s}-\tan^{-1}\frac{y-\frac{1}{2}y_s}{x-\frac{1}{2}x_s}\right), \tag{B2}$$

where b is the magnitude of the Burgers vector, σ is Poisson's ratio, x_s is the glide plane separation, and y_s is the y component of the lateral separation, here assumed equal to x_s for stability of the dipole.

If the dipole moves in the y direction with velocity $\mathbf{v}_d=v_d\hat{y}$, then $\mathbf{u}(x,y,t)=\mathbf{u}(x,y-v_dt,0)$, and the vortex-velocity field is given by $\dot{\mathbf{u}}(x,y,t)=v_d\partial\mathbf{u}(x,y,t)/\partial y$. At time $t=0$, the velocity field is thus given by the components

$$\dot{u}_x(x,y,0)=\frac{(1-2\sigma)bv_d}{4\pi(1-\sigma)}\left(\frac{(y+\frac{1}{2}y_s)}{(x+\frac{1}{2}x_s)^2+(y+\frac{1}{2}y_s)^2}-\frac{(y-\frac{1}{2}y_s)}{(x-\frac{1}{2}x_s)^2+(y-\frac{1}{2}y_s)^2}\right)+\frac{bv_d}{2\pi(1-\sigma)}\left(\frac{(y+\frac{1}{2}y_s)(x+\frac{1}{2}x_s)^2}{[(x+\frac{1}{2}x_s)^2+(y+\frac{1}{2}y_s)^2]^2}-\frac{(y-\frac{1}{2}y_s)(x-\frac{1}{2}x_s)^2}{[(x-\frac{1}{2}x_s)^2+(y-\frac{1}{2}y_s)^2]^2}\right), \tag{B3}$$

$$\dot{u}_y(x,y,0)=-\frac{bv_d}{4\pi(1-\sigma)}\left(\frac{(x+\frac{1}{2}x_s)[(x+\frac{1}{2}x_s)^2-(y+\frac{1}{2}y_s)^2]}{[(x+\frac{1}{2}x_s)^2+(y+\frac{1}{2}y_s)^2]^2}-\frac{(x-\frac{1}{2}x_s)[(x-\frac{1}{2}x_s)^2+(y-\frac{1}{2}y_s)^2]}{[(x-\frac{1}{2}x_s)^2+(y-\frac{1}{2}y_s)^2]^2}\right)$$
$$+\frac{bv_d}{2\pi}\left(\frac{x+\frac{1}{2}x_s}{(x+\frac{1}{2}x_s)^2+(y+\frac{1}{2}y_s)^2}-\frac{x-\frac{1}{2}x_s}{(x-\frac{1}{2}x_s)^2+(y-\frac{1}{2}y_s)^2}\right). \quad \text{(B4)}$$

The velocity field at arbitrary time t is given by $\dot{\mathbf{u}}(x,y,t)=\dot{\mathbf{u}}(x,\,y-v_dt,\,0)$.

The measured voltage produced by the moving FLD dipole may be expressed with the help of Eq. (4.11) in terms of the vortex-velocity field:

$$V_{ab}=\int d^2\rho\,\mathfrak{F}(\boldsymbol{\varrho},t)\cdot\nabla F_{ab}(\boldsymbol{\varrho})$$
$$=\langle n\rangle\int d^2\rho\,\dot{\mathbf{u}}(\boldsymbol{\varrho},t)\cdot\nabla F_{ab}(\boldsymbol{\varrho}). \quad \text{(B5)}$$

Since the velocity field is well localized in the vicinity of the dipole, $\nabla F_{ab}(\boldsymbol{\varrho})$ may be replaced to good approximation by its value at $\boldsymbol{\varrho}=\mathbf{v}_dt$. After performing the remaining integration, we may express the result as

$$V_{ab}\approx\langle n\rangle bx_s\partial F_{ab}(\mathbf{v}_dt)/\partial t, \quad \text{(B6)}$$

the result quoted as Eq. (4.49).

In the absence of dipole pinning, the terminal dipole speed v_d may be related to the applied transport current density $\mathbf{J}$ by a procedure similar to that used by Kramer for a screw dislocation dipole.[13] We assume that a uniform current density in the negative x direction, $\mathbf{J}=-J\hat{x}$, produces a force per unit length on a single vortex given by $\mathbf{F}=\mathbf{J}\times\boldsymbol{\varphi}_0/c=(J\varphi_0/c)\hat{y}$. The power per unit length which must be supplied by the battery to drive the dipole with speed v_d is thus

$$P=(J\varphi_0/c)\langle n\rangle\int d^2\rho\,\dot{u}_y(\boldsymbol{\varrho},t)=(J\varphi_0/c)\langle n\rangle bx_sv_d. \quad \text{(B7)}$$

This power must be equated to the dissipation per unit length arising from the viscous motion of the individual vortices,

$$D=\eta\langle n\rangle\int d^2\rho\,\dot{\mathbf{u}}^2(\boldsymbol{\varrho},t)=\eta_dv_d^2, \quad \text{(B8)}$$

where η is the viscosity coefficient appropriate to the motion of a single vortex[17] and η_d is an effective viscosity coefficient for a FLD dipole described by the parameters b and x_s. Following Kramer, we approximate this dissipation by twice the power dissipated by an isolated edge dislocation in a cylinder of diameter $x_s\sqrt{2}$, the actual separation between the two dislocations making up the dipole. To handle the logarithmic divergence of the integral very close to the edge dislocation, the integral is cut off at a radius $r_0\sim b$. This approximation leads to a terminal dipole velocity given by

$$v_d=\langle n\rangle bx_sJ\varphi_0/\eta_dc, \quad \text{(B9)}$$

where

$$\eta_d=\eta\left(\frac{\langle n\rangle b^2}{8\pi}\right)\frac{(5-12\sigma+8\sigma^2)}{(1-\sigma^2)}\ln(x_s/r_0\sqrt{2}). \quad \text{(B10)}$$

[17] Y. B. Kim, C. F. Hempstead, and A. R. Strnad, Phys. Rev. **139**, 1163 (1965).